

Supramolecular Steric Effects as the Means of Making Reactive Carbon Radicals Persistent. Quantitative Characterization of the External Surface of MFI Zeolites through a Persistent Radical Probe and a Langmuir Adsorption Isotherm[†]

Takashi Hirano,^{‡,§} Wei Li,[‡] Lloyd Abrams,^{||} Paul J. Krusic,^{||} M. Francesca Ottaviani,[⊥] and Nicholas J. Turro^{*,‡}

Department of Chemistry, Columbia University, New York, New York 10027, E. I. duPont de Nemours and Co., Central Research Department, Experimental Station, Wilmington, Delaware 19880, and University of Urbino, Institute of Chemical Sciences, Piazza Risorgimento, 6, 61029 Urbino, Italy

Received August 17, 1999

The photochemistry of tetraphenylacetone (**1**) adsorbed on the external surface of a MFI zeolite (the sodium form of LZ-105) has been investigated in combination with computational chemistry, surface area measurements, EPR analysis, and classical adsorption isotherms. All of the methods are consistent with a supramolecular structural model in which **1** is first adsorbed strongly through intercalation of a single benzene ring into a hole on the LZ-105 external surface (site I) followed by a weaker binding to the external framework between the holes (site II) until a monolayer of **1** is formed. From both computational and surface area measurements, it is estimated that the site I holes on the external surface will be filled at ca. 0.3–0.5 wt %/wt loading of **1**/LZ-105, which corresponds to 6.5×10^{18} (ca. 10^{-5} mol) of holes or molecules of **1** adsorbed in holes per gram of zeolite. The supramolecular composition of ca. 0.3–0.5% of **1** on LZ-105 characterizes a “break point” for the photochemistry and the EPR measurements, since it represents the value for saturation of the site I holes with **1**. These conclusions are supported quantitatively by experimental isotherms of the adsorption of **1** on LZ-105. Photolysis of **1** intercalated in the site I holes causes fragmentation into two isomeric supramolecular diphenylmethyl (DPM) radicals, one (DMP)_{in} which is adsorbed into the internal surface and becomes strongly persistent (half-life of many weeks) and the other (DMP)_{ex} which diffuses on the external surface and rapidly dimerizes (less than a few minutes) to produce the radical–radical combination product tetraphenylethane (**2**). Photolysis of **1** adsorbed on the solid external surface produces two supramolecularly equivalent DPM radicals (DMP)_{ex} that diffuse on the external surface and rapidly dimerize to produce **2**, and do not produce persistent DPM radicals.

Introduction

Radical Stability and Radical Persistence. The discovery of triphenylmethyl (TPM) by Gomberg in 1900 launched the field of “carbon-centered” free radical chemistry.¹ TPM exists in measurable equilibrium with its dimer, which allows for its direct observation by EPR spectroscopy in fluid solution at room temperature. This feature of TPM has caused chemists to classify TPM as a “stable” radical. Ingold has differentiated the concept of “stability” and “persistence” of carbon-centered radicals.² “Stability” is the term recommended for a radical R• that is associated with a R–H bond strength that is less than a comparable C–H bond strength in a comparable alkane, i.e., a thermodynamic definition characterizes radical stability. On the other hand, “persistence” is suggested for a radical R• when the R• has a lifetime significantly greater than that of a comparable radical

such as methyl radical CH₃• under the same conditions, i.e., a kinetic definition characterizes radical persistence. Using these criteria, TPM may be characterized as being both “stable” and “persistent”.

In ordinary solutions, the persistence of a carbon-centered radical is determined by physical processes such as diffusion, as well as chemical processes such as the rate of radical–radical reactions. As a first and good approximation, the persistence of a carbon-centered radical in fluid solution at room temperature in an inert, deaerated, solvent is determined only by the rate of radical–radical reactions (combination and disproportionation), and these are often diffusion-controlled bimolecular reactions. Ingold² has argued that the persistence of most carbon-centered radicals is primarily a consequence of *intramolecular steric* factors that slow radical–radical reactions. Indeed, in achieving persistence through steric interactions, severely twisted triaryl radicals, such as TPM, sacrifice most of the resonance stabilization energy due to electron delocalization.

Ingold's ideas concerning *intramolecular steric effect* have proven to be effective in the synthetic design of persistent carbon-centered radicals.^{2,3} In this report we employ the ideas⁴ of *supramolecular chemistry* for the

* To whom correspondence should be addressed.

[†] E. I. duPont de Nemours and Co. contribution no. 7931.

[‡] Columbia University.

[§] Present address: The University of Electro-Communications, Department of Applied Physics and Chemistry, Chofu, Tokyo 182, Japan.

^{||} E. I. duPont de Nemours and Co.

[⊥] University of Urbino.

(1) Gomberg, M. *Ber.* **1900**, *33*, 3150–3163; *J. Am. Chem. Soc.* **1900**, *22*, 757–771.

(2) Griller, D.; Ingold, K. U. *Acc. Chem. Res.* **1976**, *9*, 13–19.

(3) McBride, J. M. *Tetrahedron* **1974**, *30*, 2009–2022.

(4) Lehn, J. M. *Supramolecular Chemistry*; VCH: New York, 1995.

synthetic design of carbon-centered radicals that are rendered persistent by intermolecular, rather than intramolecular factors, i.e., *supramolecular steric effects*. The first goal of our studies is to design supramolecular persistence for benzyl and related radicals that are very reactive in solution at room temperature (i.e., those which manifest diffusion-controlled, radical–radical reactivity in “molecular” solutions). In addition, we seek conditions for which radical diffusion is allowed but for which supramolecular steric effects greatly inhibit the rate of radical–radical reactions, thereby creating radical persistence.

Zeolites as Supramolecular Environments for Reactive Carbon-Centered Radicals. Zeolites are fascinating materials for industrial purposes such as molecular sieves and catalysts.^{5–8} From the standpoint of supramolecular chemistry,⁴ zeolites possess a well-organized, crystalline, “hard matter” microenvironment for performing chemical reactions, namely the rigid aluminosilicate external and internal framework. However, in addition to the “hard” walls provided by the zeolite framework, zeolites possess “soft” void space (i.e., holes, channels, intersections) that is available for the adsorption of molecules possessing appropriate steric size/shape characteristics. In this study we employ as a supramolecular host the sodium form of LZ-105, a zeolite possessing the MFI topology. The latter topology possesses an interconnected three-dimensional void space consisting of pores and channels of ca. 5.5 Å diameter (Figure 1a,b), and intersections of ca. 9 Å diameter.^{9,10} As supramolecular guests, we have derivatives of dibenzyl ketones which, upon photolysis, produce benzyl that fits in the “soft” holes of the external surface and can diffuse within the internal channels and intersections of the internal framework at room temperature.^{11–17}

An important requirement for persistence of a mobile guest radical in a supramolecular environment is that it does not possess a significant chemical reactivity with

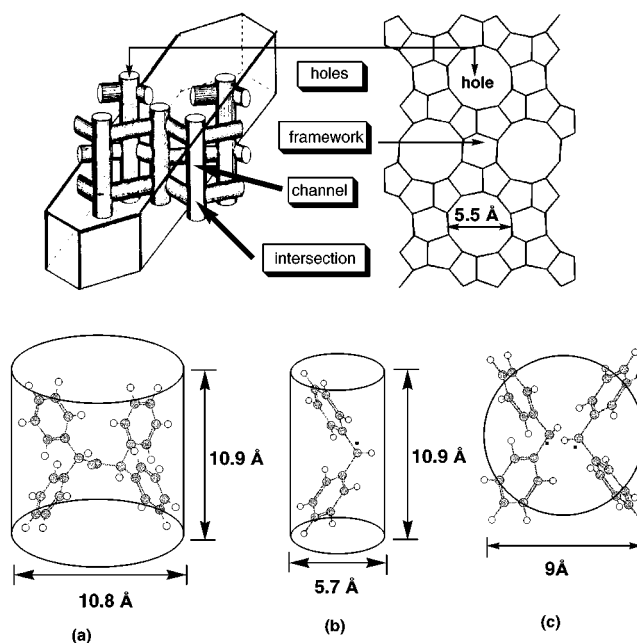
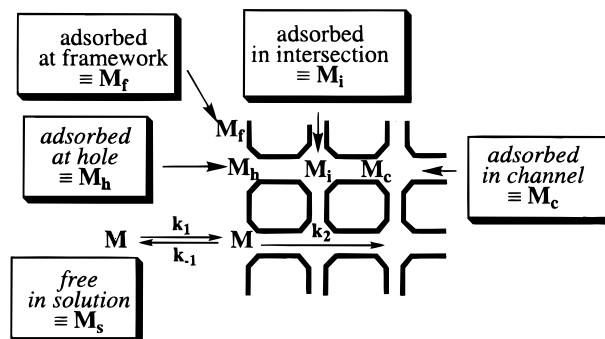


Figure 1. Schematic representation of the channel structure in a crystal and the hole structure of the [001] external surface of the MFI zeolite (top), and the molecular dimension of **1** (a), DPM (b), and two DPM radicals (c).

Scheme 1



the host. This is the case for MFI zeolites as hosts, since the framework of these zeolites consists of strong SiOSi and SiOAl bonds. Furthermore, if the cation that compensates the negative charge associated with the Al atom is sodium, there generally is not a Lewis acid effect for hydrocarbon radicals, although at some point the electron-donating capability of a radical may become significant and cations may result.

A Model for Adsorption of Organic Molecules onto MFI Zeolites. A working model for adsorption of an organic molecule, **M**, onto a MFI zeolite is shown schematically in Scheme 1. In the first step of adsorption, a molecule **M_s** is adsorbed from solution (the solvent, isooctane, was selected since it is not adsorbed into the internal framework channel network) onto one of two sites of the external surface: either a hole (**M_h**) or the external framework (**M_f**). The holes and external framework are termed the “external surface”. The model assumes that adsorption is dynamic (Figure 1, *k*₁, *k*₋₁, the rates of adsorption at the sites on the surface need not be equal) and reaches an equilibrium between adsorption at the two sites and the solution in contact with the zeolite. The internal channels and intersections (Scheme 1) are termed collectively as the internal surface.

(5) Davis, M. E.; Lobo, R. F. *Chem. Mater.* **1992**, *4*, 756–768.

(6) Meier, W. M.; Olson, D. H. *Atlas of Zeolite Structure Types*; Butterworth-Heinemann: London, 1992.

(7) Breck, D. W. *Zeolite Molecular Sieves: Structure, Chemistry, and Use*; Wiley and Sons: London, 1974.

(8) Szostak, R. *Molecular Sieves: Principle of Synthesis and Identification*; Van Nostrand Reinhold: New York, 1989.

(9) (a) Kokotailo, G. T.; Lawton, S. L.; Olson, D. H.; Meier, W. M. *Nature (London)* **1978**, *272*, 437–438. (b) Olson, D. H.; Kokotailo, G. T.; Lawton, S. L.; Meier, W. M. *J. Phys. Chem.* **1981**, *85*, 2238–2243.

(10) Flanigen, E. M.; Bennet, J. M.; Grose, R. W.; Cohen, J. P.; Patton, R. L.; Kirchner, R. M.; Smith, J. V. *Nature (London)* **1978**, *272*, 512–516.

(11) (a) Turro, N. J.; Cheng, C.-C.; Mahler, W. *J. Am. Chem. Soc.* **1984**, *106*, 5022–5023. (b) Turro, N. J.; Cheng, C.-C.; Abrams, L.; Corbin, D. R. *J. Am. Chem. Soc.* **1987**, *109*, 2449–2456.

(12) Reviews: (a) Turro, N. J. *Pure Appl. Chem.* **1986**, *58*, 1219–1228. (b) Ramamurthy, V.; Turro, N. J. *J. Incl. Phenom. Mol. Recognit. Chem.* **1995**, *21*, 239–282.

(13) Photochemistry of dibenzyl ketone: (a) Engel, P. S. *J. Am. Chem. Soc.* **1970**, *92*, 6074–6076. (b) Robbins, W. K.; Eastman, R. H. *J. Am. Chem. Soc.* **1970**, *92*, 6076–6077. (c) Robbins, W. K.; Eastman, R. H. *J. Am. Chem. Soc.* **1970**, *92*, 6077–6079.

(14) Photochemistry of tetraphenyl acetone: (a) Quinkert, G.; Opitz, K.; Weirdorff, W. W.; Weinlich, J. *Tetrahedron Lett.* **1963**, 1863–1868. (b) Quinkert, G. *Pure Appl. Chem.* **1964**, *9*, 607–621.

(15) (a) Turro, N. J.; Gould, I. R.; Baretz, B. H. *J. Phys. Chem.* **1983**, *87*, 531–532. (b) Gould, I. R.; Baretz, B. H.; Turro, N. J. *J. Phys. Chem.* **1987**, *91*, 925–929.

(16) Lunazzi, L.; Ingold, K. U.; Scaiano, J. C. *J. Phys. Chem.* **1983**, *87*, 529–530.

(17) (a) Turro, N. J.; Lei, X.; Li, W.; McDermott, A.; Abrams, L.; Ottaviani, M. F.; Beard, H. S. *Chem. Commun.* **1998**, 695–696. (b) Turro, N. J.; McDermott, A.; Lei, X.; Li, W.; Abrams, L.; Ottaviani, M. F.; Beard, H. S.; Houk, K. N.; Beno, B. R.; Lee, P. S. *Chem. Commun.* **1998**, 697–698.

If its size/shape characteristics are appropriate, the molecule M_h will eventually diffuse (k_d) into the internal surface, leading to a molecule that is adsorbed in the internal channels (M_c) or intersections (M_i). Molecules that initially adsorb on the external framework (M_f) must first diffuse and be adsorbed into a hole in order to be adsorbed into the internal surface i.e., $M_f \rightarrow M_h \rightarrow M_i$ (or M_c). It is important to note that M_f , M_h , M_c , and M_i each corresponds to *distinct* supramolecular structures. Since these distinct supramolecular structures correspond to the same supramolecular composition, but differ with respect to the manner in which the guest is "connected to the host", these structures are *supramolecular isomers*.

Estimation of the Moles of Holes on the External Surface of MFI Zeolites. An important structural issue is whether the holes (site I) or the external framework (site II) bind a guest molecule M more strongly. It is of interest to estimate the total number of holes on the external surface in order to anticipate, experimentally, the loading at which the holes will be filled by M , i.e., to determine the maximum moles of holes, M_h , that are possible per gram of zeolite. The moles of holes may be computed quantitatively, and bounds can be placed on the number of molecules adsorbed in the holes on the external framework from the estimated or measured surface area of a MFI zeolite and knowledge of the crystalline parameters of MFI zeolites as follows.

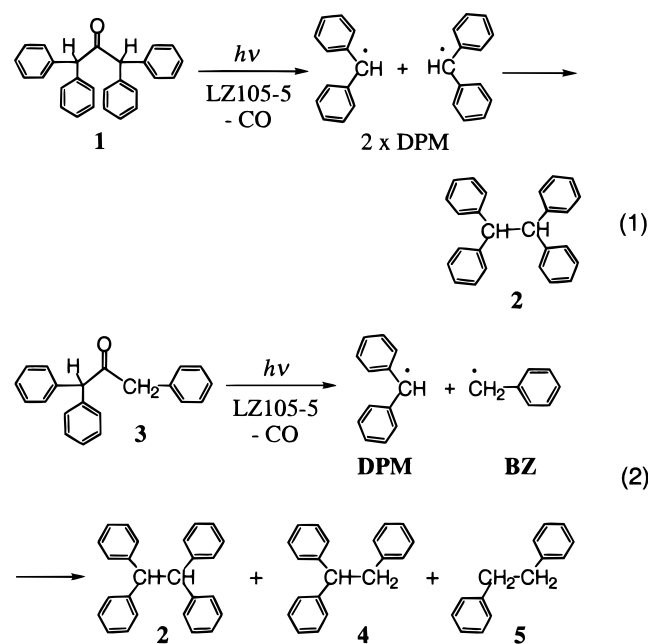
Scanning electron microscope analysis of LZ-105 reveals that the zeolite consists of crystals (particles) whose size is of the order of ca. $0.3 \mu\text{m}$. An order of magnitude estimation of the surface area of 1.0 g of the sample can be made if it is assumed that the shape of the particles is cubic. The volume of a $0.3 \mu\text{m}$ crystal is ca. $2.7 \times 10^{-20} \text{m}^3$. From the volume of a single particle and the crystal density of LZ-105 which is 1.8 g/mL ($= 1.8 \times 10^6 \text{ g m}^{-3}$), 1.0 g of LZ-105 will consist of 2.1×10^{13} particles whose external surface area is estimated to be ca. $11 \text{ m}^2 \text{ g}^{-1}$. The external surface area of samples of LZ-105 was measured directly by mercury porosimetry independently and yielded a value for the surface area of $15 \text{ m}^2 \text{ g}^{-1}$. Thus, both the estimated and experimental values of the external surface area are completely consistent with one another and provide confidence that a reliable surface area can be associated with the samples of LZ-105.

The number of holes on the LZ-105 external surface may now be estimated from knowledge of the surface area and from the dimensions of the unit cell of silicalite as a model MFI zeolite.⁹ The size of the unit cell of silicalite is $20.4 \text{ \AA} \times 20.4 \text{ \AA} \times 13.8 \text{ \AA}$, and the surface area of a unit cell is calculated to be 1960 \AA^2 . There are eight holes per unit cell, four of which are the entrance to the straight channels (Figure 1), and the other four are the entrance to the sinusoidal channels (Figure 1). Therefore, the number density is 8 holes/ 1960 \AA^2 , or 1 hole per 245 \AA^2 ($= 2.45 \times 10^{-18} \text{ m}^2$). The value 245 \AA^2 is defined as a "unit surface area" of a hole that is available to an adsorbed molecule. By using this value and the measured external surface area ($15 \text{ m}^2 \text{ g}^{-1}$), the number of holes on the external surface of this sample of LZ-105 is computed to be 6.5×10^{18} holes g^{-1} (ca. 10^{-5} mol). The fraction of external surface corresponding to site I holes is ca. 20–30%, the remaining 70–80% being the site II external framework. We are finally in a position to compute the adsorbed amount of M (molecular weight 362) to be ca. 0.4 mg per 100 mg of LZ-105 (0.3–0.5 wt %/wt loading), when all the holes were filled by M . This

loading is expected to correspond to a composition at which the supramolecular structure changes from M_f /LZ-105 to M_f /LZ-105, where the notation refers to different supramolecular isomers.

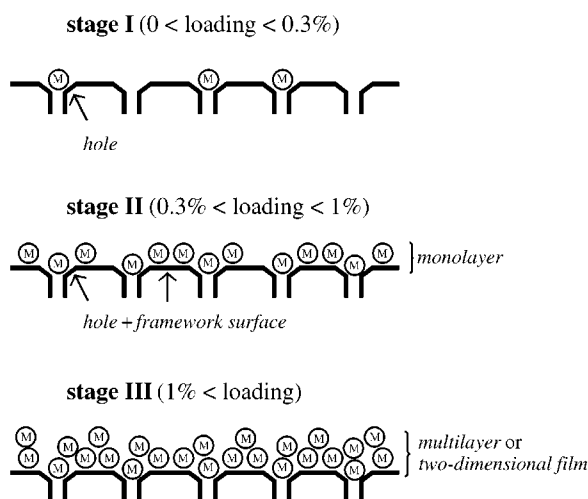
Molecular Photochemistry of 1,1,3,3-Tetraphenyl Acetone (1) and 1,1,3-Triphenyl Acetone (3). The photochemistry of dibenzyl ketone (DBK) derivatives has proven to be useful for characterizing the supramolecular structures and dynamics of molecular adsorbents and radicals produced by photolysis.^{11,12} The molecular photochemistry of DBK and its derivatives consists of adsorption of light to form a singlet, S_1 , followed by intersystem crossing and α -cleavage from a triplet T_1 to produce two benzyl radical derivatives (after rapid elimination of CO).^{13–16} The molecular photochemistry of the benzyl radicals in fluid solution consists, nearly exclusively, of diffusion-controlled radical combination reactions with a cage effect close to zero, i.e., essentially no geminate pair reactions occur. In contrast, the *supramolecular* photochemistry^{11,12} of DBK in zeolites shows substantial geminate cage effects, which can be directly related to simple ideas of "supramolecular steric effects" imposed by the supramolecular "cage" produced by the "hard walls" of the zeolite framework.

1,1,3,3-Tetraphenylacetone, **1**, and 1,1,3-triphenylacetone, **3**, were selected as precursors of diphenylmethyl radicals (DPM). These molecules were selected because their size/shape characteristics are much larger (Figure 1) than the characteristic size/shape of the holes on the external surface. **1** is photolyzed to yield 1,1,2,2-tetraphenylethane (**2**), quantitatively (eq 1), and **3** is photolyzed to yield (eq 2) a statistical mixture of **2** (25%), **4** (50%), and **5** (25%) expected from random coupling of the DPM and benzyl (BZ) radicals produced by photolysis. The molecular photochemistry of both **1** and **3** in nonviscous solution consists of formation of radicals that undergo quantitative random radical–radical coupling.



1 and **3** represent molecules, M (Scheme 1), that cannot diffuse into the internal surface. Thus, **1** and **3** can only be adsorbed at site I (holes) and site II (framework). We shall now show that the siting of **1** and **3** has profound

Scheme 2



and decisive effects on the photochemistry of these different supramolecular structures.

Application of the Model to the Photochemistry of 1. From the molecular dimensions of **1** and previous results,¹⁷ it is expected (Scheme 2) that **1** will first adsorb in the site I holes (1_h) of the external surface of LZ-105 to form a supramolecular complex, $1_h/\text{LZ-105}$. From the considerations discussed above, the holes will be filled at ca. 0.3–0.5% loading. Further adsorption beyond this composition will occur at the site II external framework to form a new supramolecular structure, $1_f/\text{LZ-105}$, until a monolayer is formed. Since the supramolecular structure of $1/\text{LZ-105}$ is expected to change at ca. 0.3–0.5% loading of **1**, it is of interest to determine if the photochemistry of $1/\text{LZ-105}$ was a function of loading and also to determine if some special photochemical effects occurred at the point expected for the completion of the filling of the holes with **1**.

From computer simulations, the $1_h/\text{LZ-105}$ species possess a structure in which one benzene ring is intercalated in a hole and the remainder of the molecule extends in a direction away from the surface. Photolysis of $1_h/\text{LZ-105}$ will produce two distinct supramolecular, isomeric diphenylmethyl radicals (DPM), one intercalated in the hole (DPM_h) and the other adsorbed on the external framework (DPM_f). The DPM_h radicals are predisposed to diffusion into the internal surface, whereas the DPM_f radicals are disposed to diffusion on the external framework. The radicals on the external framework are expected to undergo dimerization to form tetraphenylethane (**2**). However, the radicals entering the internal surface are expected to be persistent, since the largest space in the internal surface corresponds to the intersections possessing a diameter of ca. 9 Å, whereas the smaller molecular cross section of **2** is ca. 11 Å (Figure 1). We shall show below that the photochemistry of **1** and of triphenylacetone, **3**, support these supramolecular structural considerations. Furthermore, we shall show that EPR and classic adsorption isotherms quantitatively confirm the conclusion that the holes are first filled by **1** and **3** and that the holes are completely filled at ca. 0.3–0.5% loading of **1** and **3**.

Results

As expected from literature reports (see eqs 1 and 2), photolysis of **1** in solution yielded **2** in quantitative yield,

Table 1. Product Analysis of the Photoreaction of 1 Adsorbed on LZ-105

| loading, % | irradiation time/min | conversion, % | yield/% (conversion yield/%) | |
|---------------|-------------------------|------------------|------------------------------|--------------------|
| | | | 2 | Ph ₂ CO |
| 0.10 | 5 | 36 | 16 (43) | 2 |
| 0.10 | 10 | 38 | 13 (35) | 3 |
| 0.30 | 5 | 22 | 10 (44) | 1 |
| 0.30 | 10 | 30 | 13 (43) | 1 |
| 0.51 | 5 | 21 | 10 (45) | trace |
| 0.50 | 10 | 33 | 13 (40) | trace |
| 0.70 | 5 | 26 | 14 (52) | 1 |
| 0.70 | 10 | 35 | 18 (50) | trace |
| 1.10 | 5 | 27 | 15 (56) | 1 |
| 1.10 | 10 | 38 | 23 (62) | trace |

and the photolysis of **3** in *n*-hexane gave tetraphenylethane (**2**), triphenylethane (**4**), and diphenylethane (**5**) in 19, 33, and 17% yields (essentially a statistical coupling), respectively.

The photoreaction of **1**/zeolites has already been investigated by laser flash photolysis in the zeolite systems of NaX and silicalite, as well as silica gel. DPM is produced and is transient with decay times ranging over many orders of magnitude.¹⁸ The products reported were **2** and benzophenone.

Samples of **1**/LZ-105 and **3**/LZ-105 were prepared by adsorption of **1** (or **3**) onto LZ-105 from an isooctane solution, followed by removal of the bulk of the solvent by drying with a stream of argon gas followed by vacuum degassing at ca. 5×10^{-5} Torr to remove the remainder of the isooctane in order to prepare a “dry” sample.

After exposing the photolyzed **1**/LZ-105 to air, the products were extracted by soaking overnight with THF containing methanol (5% v/v) and then were analyzed by GC. The yields of the products are summarized in Table 1. Tetramethylethane **2** was obtained as the main product in ca. 40–45% yield, in addition to a trace amount of benzophenone. The yield of **2** was independent of the percentage of loading up to ca. 0.5%. Above 0.5% loading of **1** on LZ-105, the yield of **2** increased to 50–60%.

In the case of the photoreaction of **3**/LZ-105 (0.5% loading), followed by exposure to air and extraction with THF containing methanol (5% v/v) GC analysis, **2**, **4**, and **5** were the major detectable products and were formed in yields of 4, 13, and 5%, respectively.

Photolysis of 1/LZ-105 and 3/LZ-105. EPR Analysis. Irradiated samples of **1**/LZ-105 or **3**/LZ-105 exhibited strong EPR spectra (Figure 2). In the case of irradiated **1**/LZ-105 the EPR spectrum (Figure 2a) could be confidently assigned to the diphenylmethyl radical (DPM) through simulation (Figure 2d) with hyperfine coupling constants, $a_\alpha = 14.8$ G, $a_o = 3.7$ G, $a_m = 1.1$ G, $a_p = 4.1$ G (Figure 2d) comparable to reported values.^{19,20} The EPR signals of DPM were persistent for many days under vacuum at room temperature, and sharpened slightly with time (Figure 2b), indicating that the radicals moved from the internal surface sites of lower mobility (e.g., the channels of the internal framework) to sites of higher mobility (e.g., the intersections of the internal frame-

(18) (a) Kelly, G.; Willsher, C. J.; Wilkinson, F.; Netto-Ferreira, J. C.; Weir, A. O. D.; Johnston, L. J.; Scaiano, J. C. *Can. J. Chem.* **1990**, *68*, 812–819. (b) Johnston, L. J.; Scaiano, J. C.; Shi, J.-L.; Siebrand, W.; Zerbetto, F. *J. Phys. Chem.* **1991**, *95*, 10018–10024.

(19) Bassindale, A. R.; Bowles, A. J.; Hudson, A.; Jackson, R. A.; Schreiner, K.; Berndt, A. *Tetrahedron Lett.* **1973**, 3185–3186.

(20) Livingston, R.; Zeldes, H.; Conradi, M. S. *J. Am. Chem. Soc.* **1979**, *101*, 4312–4319.

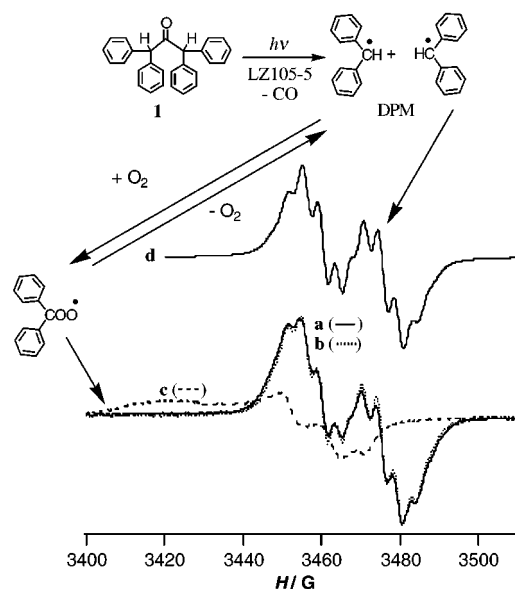


Figure 2. EPR spectra (a, b, c) of the products of the photoreaction of **1** adsorbed on LZ-105. Spectra a and b of DPM were observed under degassed conditions 5 min and 5 h after irradiation of **1** for 10 min, respectively. Spectrum c was observed 1 min after exposing the DPM sample to air. The simulated spectrum d was calculated by using the parameters in the text.

work). Upon exposure of the sample to air, the signals of DPM immediately disappeared and were replaced with a new spectrum possessing a larger g-factor and anisotropy (Figure 2). This new species is assigned to a peroxy radical (Figure 2c).²¹ The EPR signal of the peroxy radical gradually decreased at room temperature. Formation of the peroxy radical is reversible: if the sample is subjected to a vacuum, the spectrum of the DPM radical reappears, replacing the spectrum of the peroxy radical.

An irradiated sample of **3**/LZ-105 under degassed conditions also exhibits strong EPR signals (Figure 3). For **1**, except for a small amount of broadening, the spectral features of the EPR spectrum were constant with time. However, the EPR spectrum produced from the photolysis of **3** changed significantly with time. After 5 h, the EPR spectrum (Figure 3b) matched the spectra of DPM obtained by the photoreaction of **1**/LZ-105 (Figure 2a,b). Evidently, one (or more) radicals in addition to DPM is produced by photolysis of **3**; the EPR of this other radical can be detected along with that of DPM, but the radical is not as persistent as DPM. The obvious candidate for a transient radical is the benzyl radical (BZ), which is expected to be produced (eq 2) along with DPM in the photolysis of **3**. Indeed, subtraction of the spectrum in Figure 3b (5 h after photolysis) from Figure 3a (5 min after photolysis) yields the spectrum shown in Figure 3c. Figure 3d shows the spectrum of BZ, simulated from the reported hyperfine coupling constants; $a_n = 16.4$ G, $a_o = 6.2$ G, $a_m = 1.8$ G, $a_p = 5.2$ G (Figure 3d).^{20,22–24} Agreement between the simulated (Figure 3d) and subtracted spectrum (Figure 3c), together with expectation of the radical products from photolysis of **3** leave no doubt that Figure 3a represents a mixture of BZ and DPM radicals.

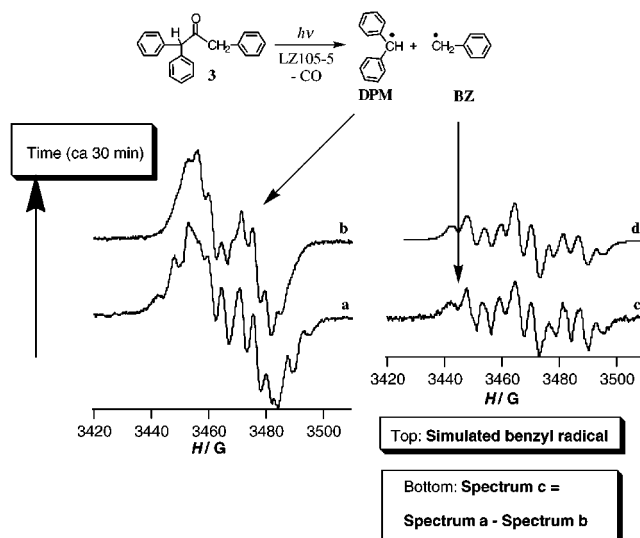


Figure 3. EPR spectra (a, b, c) of the product of the photoreaction of **3** adsorbed on LZ-105. Spectra a and b of the radicals observed under degassed conditions 5 min and 5 h after irradiation of **3** for 10 min, respectively. Spectrum c was obtained by subtracting b from a. The simulated spectrum d of benzyl radical was calculated by using the parameters in the text.

From the time dependence of the conversion of Figure 3a to Figure 3b, it is estimated that the benzyl radicals produced from photolysis of **3**/LZ-105 possess a half-life of ca. 40 min at room temperature, a time scale for which DPM is completely persistent. From a quantitative evaluation of the EPR signal intensities of DPM produced from photolysis of **1** and **3**, it was estimated that the amount of DPM generated from **3** on LZ-105 was approximately half of the amount of DPM from **1** on LZ-105.

Time-Dependence of the Generation of Persistent DPM from the Photoreaction of Tetraphenylacetone on LZ-105 as a Function of Loading. The above product and EPR analyses provide evidence that the working model for the photolysis of **1**/LZ-105 and **3**/LZ-105 (Schemes 1 and 2) is valid and that the holes are filled first and are saturated with **1** and **3** at ca. 0.3–0.5% loading. Further support for the model is available from a quantitative investigation of the time dependence of the EPR signal intensity of DPM radicals produced by photolysis of **1**.

Figure 4 shows the time dependence of the generation of DPM as a function of the percentage of loading of **1** on LZ-105. Figure 5 shows that the EPR signal intensities of the persistent DPM obtained by irradiation for 10, 30, and 90 min correlated with the percentage of loading of **1** on LZ-105. However, a clear break in the sensitivity of the signal intensity to loading occurs at ca. 0.3–0.5% loading. For example, in the case of 0.1% loading, the yield of DPM reached the maximum by irradiation for 40 min and gradually decreased with longer irradiation over 40 min. Above 0.2% loading, the maximum amount of DPM was obtained by irradiation around 90 min. Importantly, the amount of the persistent DPM linearly increased with an increase in the loading amount of **1** below 0.3–0.5% loading (Figure 5). Significantly, above 0.3–0.5% loading, the amount of the persistent DPM increased only slightly with an increase in the percentage of loading of **1**. The results of 90 min irradiation shown

(21) Schlick, S.; Kevan, K. *J. Phys. Chem.* **1979**, *83*, 3424–3429.

(22) Dixon, W. T.; Norman, R. O. C. *J. Chem. Soc.* **1964**, 4857–4860.

(23) Fischer, H. *Z. Naturforsch. A* **1965**, *20*, 488–489.

(24) Neta, P.; Schuler, R. H. *J. Phys. Chem.* **1973**, *77*, 1368–1370.

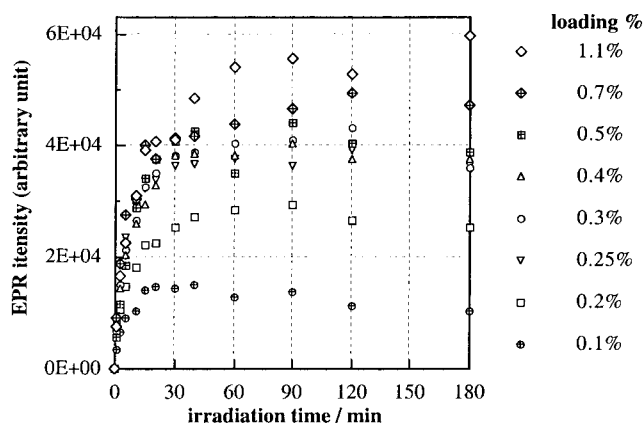


Figure 4. Time-course of the generation of DPM by the photoreaction of **1** adsorbed on LZ-105 with various loading amounts.

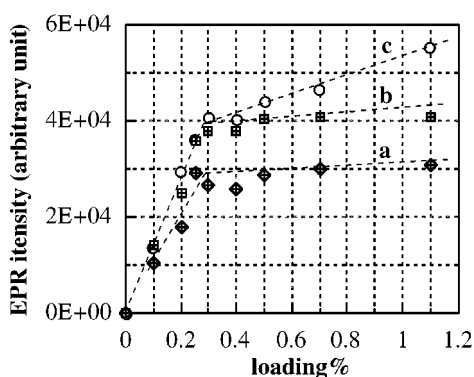


Figure 5. The EPR signal intensity of DPM generated by irradiation of **1**/LZ-105 for 10 (a), 30 (b), and (c) 90 min vs loading percentage of **1** on LZ-105.

in Figure 5c shows that the slope above 0.3–0.5% loading was steeper than the others. These results are consistent with the working model: the supramolecular structure of **1**/LZ-105 changes from 1_h /LZ-105 to 1_f /LZ-105 at loading of ca. 0.3–0.5%, the point at which the holes on the external surface are becoming completely filled. After this point, further adsorption of TPM begins to occur on the solid framework between the holes. It may be concluded at this point that photolysis of 1_f /LZ-105 produces DPM_f that diffuse and combine to form **2** on the external surface rather than be adsorbed into the internal surface to form persistent DPM radicals.

Langmuir Isotherms for the Adsorption of Tetraphenylacetone (1) Adsorbed on LZ-105. Having obtained photochemical and EPR evidence for the working model, we add further support through Langmuir isotherm analysis of the adsorption of **1**, **3**, and other model compounds on LZ-105.

Adsorption of the molecules on the LZ-105 external and internal surfaces may be evaluated quantitatively by a Langmuir isotherm analysis.²⁵ In a typical experiment, **1** was adsorbed on 100 mg of LZ-105 from an isooctane solution of **1** (1.0 mg of **1** in 3 mL of isooctane) at room temperature. The time dependence of the adsorption of **1** is shown in Figure 6. Under these conditions, the adsorption of **1** on LZ-105 from the isooctane solution

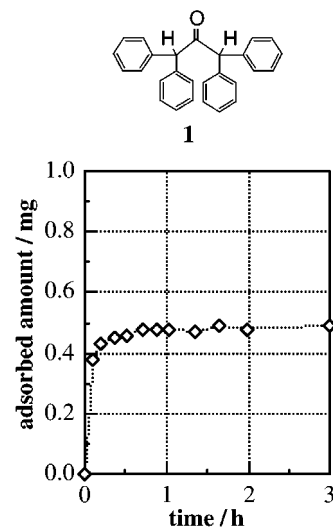


Figure 6. Time-course of the adsorbed amount of **1** on 100 mg of LZ-105 from an isooctane solution of **1** (initial concentration: 1.0 mg of **1** in 3 mL).

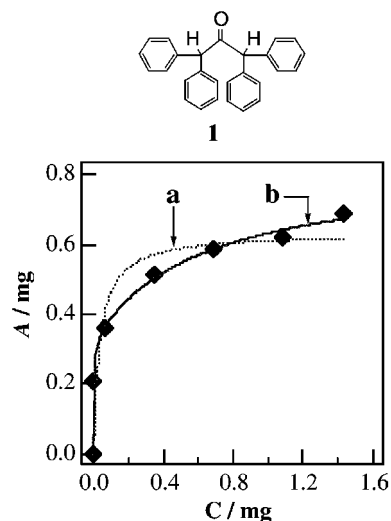


Figure 7. Langmuir isotherm analysis of **1** adsorbed on the LZ-105 surface from an isooctane solution. *A* (*y* axis) is the amount (mg) of **1** adsorbed on 100 mg of LZ-105 at equilibrium, and *C* (*x* axis) is the amount (mg) of **1** left in a 3 mL solution. Curves a and b were calculated by using the Langmuir isotherm eqs 1 and 2 in the text, respectively.

reached equilibrium in ca. 40 min. The Langmuir isotherm for adsorption of **1** on LZ-105 consists of a plot (Figure 7) of the amount of **1** remaining in solution (*x*-axis) versus the amount of **1** adsorbed on 100 mg of LZ-105 at equilibrium (*y*-axis). An attempt (Figure 7a) was made to fit the experimental data (Figure 7b) to the one site Langmuir isotherm (eq 3)

$$A = MkC/(1 + kC) \quad (3)$$

where *A* is the amount (mg) of adsorbate adsorbed on 100 mg of LZ-105 at equilibrium, *M* is the maximum amount adsorbed on 100 mg of LZ-105 at equilibrium, *k* is the Langmuir constant that is related to an equilibrium constant, and *C* is the amount (mg) of adsorbate left in 3 mL of solution at equilibrium. It is clear from Figure 7a, that a single site model does not give a good fit to the data.

(25) Oscik, J.; Cooper, I. L. *Adsorption*; Ellis Horwood Ltd, Chichester, 1982.

Table 2. Langmuir Isotherm Analysis of the Adsorption of 1, 3, 6, and 7 on LZ-105 from Isooctane Solutions by Using the Two-Adsorption Site Model

A: Calculated by Using the Value of the Adsorbed Amount (mg) on 100 mg of LZ-105

| ketone | site I | | site II | |
|----------|-------------|-----------|---------------|-----------|
| | M_I , mg | k_I | M_{II} , mg | k_{II} |
| 1 | 0.33 ± 0.03 | 300 ± 100 | 0.50 ± 0.05 | 1.6 ± 0.7 |
| 3 | 0.4 ± 0.2 | 200 ± 400 | 0.6 ± 0.2 | 1 ± 2 |
| 6 | 0.40 ± 0.02 | 350 ± 50 | 0.59 ± 0.02 | 2.1 ± 0.3 |
| 7 | 0.25 ± 0.03 | 120 ± 50 | 0.49 ± 0.07 | 0.8 ± 0.4 |

B: Calculated by Using the Value of Adsorbed Amount (mol) per "Unit Surface Area" of LZ-105

| ketone | site I | | site II | |
|----------|-------------|-----------------------|----------------|----------------------|
| | M_I , mol | k_I | M_{II} , mol | k_{II} |
| 1 | 0.93 ± 0.01 | $(10.8 ± 0.6) × 10^7$ | 1.52 ± 0.02 | $(4.1 ± 0.3) × 10^5$ |
| 3 | 1.3 ± 0.1 | $(7 ± 2) × 10^7$ | 1.90 ± 0.07 | $(3.2 ± 0.9) × 10^5$ |
| 6 | 1.74 ± 0.01 | $(8.0 ± 0.2) × 10^7$ | 2.51 ± 0.01 | $(5.1 ± 0.1) × 10^5$ |
| 7 | 1.01 ± 0.02 | $(3.0 ± 0.2) × 10^7$ | 1.91 ± 0.02 | $(2.2 ± 0.1) × 10^5$ |

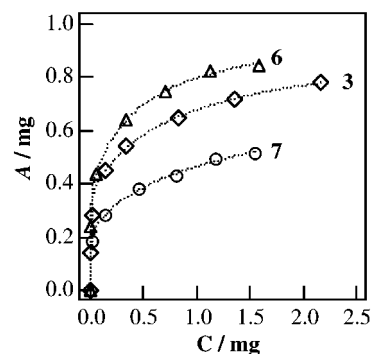
However, since the paradigm of Schemes 1 and 2 suggests that there should be two sites of differing binding energies (the holes and the solid surface), it is natural to expect that a two-site model, rather than a one-site model is required to fit the experimental data. Therefore, we modified the Langmuir isotherm to take this inference into account and applied the data to eq 4

$$A = M_I k_I C / (1 + k_I C) + M_{II} k_{II} C / (1 + k_{II} C) \quad (4)$$

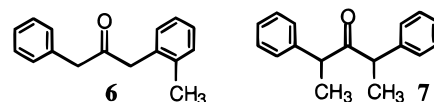
where sites I and II have the maximum amounts adsorbed on LZ-105 at equilibrium M_I and M_{II} and the Langmuir constants k_I and k_{II} , respectively. Figure 7b shows that, as expected from the two-site model, eq 4 provides an excellent fit to the experimental data. The values of M_I , M_{II} , k_I , and k_{II} were obtained from the fitting curve **b** as summarized in Table 2A and, according to Scheme 1, provide quantitative information on the binding strengths and fractions of **1** molecules bound in the two sites, i.e., the supramolecular structure of the external surface of **1**/LZ-105. We are now in a position to test this expectation quantitatively and to then correlate the results with the photochemical and EPR results.

From Langmuir analysis, the binding constant, k_I , of site I is a hundred times larger than k_{II} of site II, indicating that site I has a much stronger adsorption affinity for **1** than site II on the LZ-105 external framework surface. According to the working model, site I is the holes on the external surface and site II is the solid framework between the holes. From Langmuir analysis, the maximum amount of **1** adsorbed on site I of the LZ-105 surface is ca. 0.3 mg per 100 mg of LZ-105, which corresponds to 0.3–0.5% loading, experimentally consistent with the loading expected for filling the holes from both computation and the results of photochemical and EPR analysis. Thus, a quantitative working model of Schemes 1 and 2 are supported by excellent agreement between data from several independent sources: theoretical computations, photochemical product analysis, EPR analysis, and classical isotherm analysis.

Langmuir Isotherms for the Adsorption of Derivatives of Tetraphenylacetone and Related Structures Adsorbed on LZ-105. Given the above results, it appears that classical Langmuir analysis is capable of providing information on the supramolecular structure of molecules adsorbed on the external surface of LZ-105.

**Figure 8.** Langmuir isotherm analysis of **3**, **6**, and **7** adsorbed on the LZ-105 surface from an isooctane solution.

This finding led us to expect that correlations could be found between the molecular structure of adsorbed molecules and the supramolecular binding parameters extractable from a Langmuir analysis. Although **3** and dibenzyl ketone derivatives **6** and **7** have larger molecular cross sections (ca. 6–7 Å) than the diameters of the channels of LZ-105, as for **1**, the benzene (ca 5 Å) portion of the molecular structures of **3**, **6**, and **7** can fit into the holes on the external surface. Thus, it is expected that **3**, **6**, and **7** will possess Langmuir isotherms that fit the two-site model for adsorption on the external surface.



Indeed, isotherms for adsorption of **3**, **6**, and **7** were well fitted by eq 4 (Figure 8). Adsorption constants extracted from eq 4 are summarized in Table 2A. The binding constants for **3**, **6**, and **7** were similar to those of **1**, supporting evidence for the existence of two adsorption sites which are structurally similar for this class of DBK derivatives: site I (holes) which have ca. 100 times stronger adsorption ability for the benzene moiety of each molecule than does site II (solid surface). The constants M_I , M_{II} , k_I , and k_{II} were also described as the values M_I , M_{II} , k_I , and k_{II} . The data in Table 2B are also expressed in terms of a "unit surface area" as a unit of 245 Å², which is the area of a hole.

Time Dependence of the Adsorption of Diphenylmethane and Related Structures on LZ-105. Adsorption of diphenylmethane, **8**, on LZ-105 was employed as an isosteric model for DPM in Langmuir studies. In addition, *o*-xylene (**9**), *p*-xylene (**10**), triphenylmethane (**11**), acetophenone (**12**), and 2'-methylacetophenone (**13**) were studied as model compounds to investigate specific molecular structural features of adsorption on LZ-105. *p*-Xylene and acetophenone were employed as model small molecules (hydrocarbon and ketone) which should be readily adsorbed into the internal surface of LZ-105.^{9,26–28} On the other hand, *o*-xylene, triphenylmethane, and 2'-methylacetophenone were used as model sterically bulky molecules, in the supramolecular sense, which cannot be adsorbed into the internal surface of LZ-105,

(26) van Koningsveld, H.; Tuinstra, F.; van Bekkum, H.; Jansen, J. C. *Acta Crystallogr., Sect. B* **1989**, *B45*, 423–431.

(27) Fyfe, C. A.; Strobl, H.; Kokotailo, G. T.; Kennedy, G. J.; Barlow, G. E. *J. Am. Chem. Soc.* **1988**, *110*, 3373–3380.

(28) Reischman, P. T.; Schmitt, K. D.; Olson, D. H. *J. Phys. Chem.* **1988**, *92*, 5165–5169.

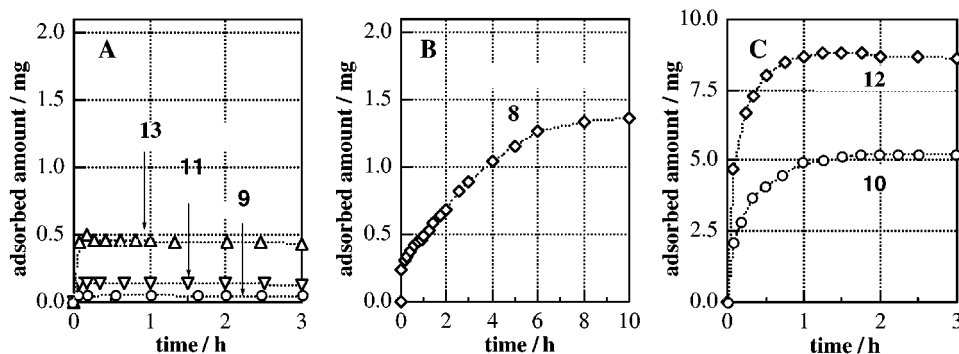


Figure 9. Adsorption time-course of diphenylmethane and its related compounds on 100 mg of LZ-105 from an isooctane solution. The time-course (A) for *o*-xylene (**9**), triphenylmethane (**11**), and 2'-methylacetophenone (**13**) (initial concentration: 2.1 mg in 3 mL); the time-course (B) for diphenylmethane (**8**) (initial concentration: 2.1 mg in 3 mL); and the time-course (C) for *p*-xylene (**10**) and acetophenone (**12**) (initial concentration: 10.0 mg in 3 mL).

Scheme 3

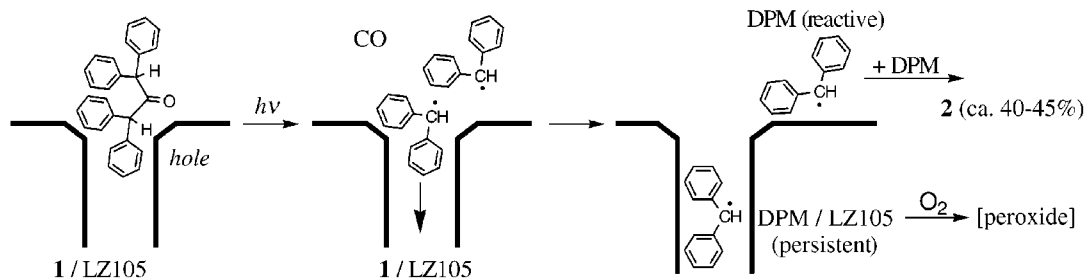


Table 3. Langmuir Isotherm Analysis of the Adsorption of Diphenylmethane-Related Compounds on 100 mg of LZ-105 from Isooctane Solutions^a

| compound | <i>M</i> , mg | <i>k</i> |
|-----------------------|---------------|-----------|
| triphenylmethane | 0.19 ± 0.01 | 4 ± 1 |
| <i>p</i> -xylene | 4.6 ± 0.2 | 130 ± 30 |
| <i>o</i> -xylene | 0.05 | <i>b</i> |
| acetophenone | 9.5 ± 0.3 | 90 ± 20 |
| 2'-methylacetophenone | 0.59 ± 0.01 | 2.4 ± 0.2 |

^a Constants *M* and *k* were calculated by using the Langmuir equation 3.

but which contain a benzene ring that can be adsorbed in the holes on the external surface. The adsorption of **8–13**, as a function of time, on LZ-105 (100 mg) from isooctane solutions at room temperature is shown in Figure 9. For the results in Figure 9, the initial concentrations of diphenylmethane, *o*-xylene, triphenylmethane, and 2'-methylacetophenone were 2.1 mg/3 mL, respectively, and for *p*-xylene and acetophenone, the initial concentrations were 10.0 mg/3 mL, respectively. In the case of *o*-xylene, triphenylmethane, and 2'-methylacetophenone, adsorption reached an equilibrium in 10 min (Figure 9a). In the case of *p*-xylene and acetophenone, a fast adsorption was observed in 10 min followed by a slower adsorption, with equilibrium being achieved in ca. 2 h (Figure 9c). Diphenylmethane also showed a fast adsorption process in 10 min, but then adsorption increased relatively slowly and linearly achieving a maximum amount in 10 h (Figure 9b).

Adsorption properties of compounds **8–13** were also analyzed using a Langmuir isotherm analysis. In contrast to the results for **1**, **3**, **6**, and **7**, for which eq 4 was required for a good fit, the isotherms for the other molecules, with the exception of *o*-xylene, were fitted by using eq 3, and the *M* and *k* values were summarized in Table 3. The Langmuir constants *k* of *o*-xylene could not be determined, because of its low adsorption ability on

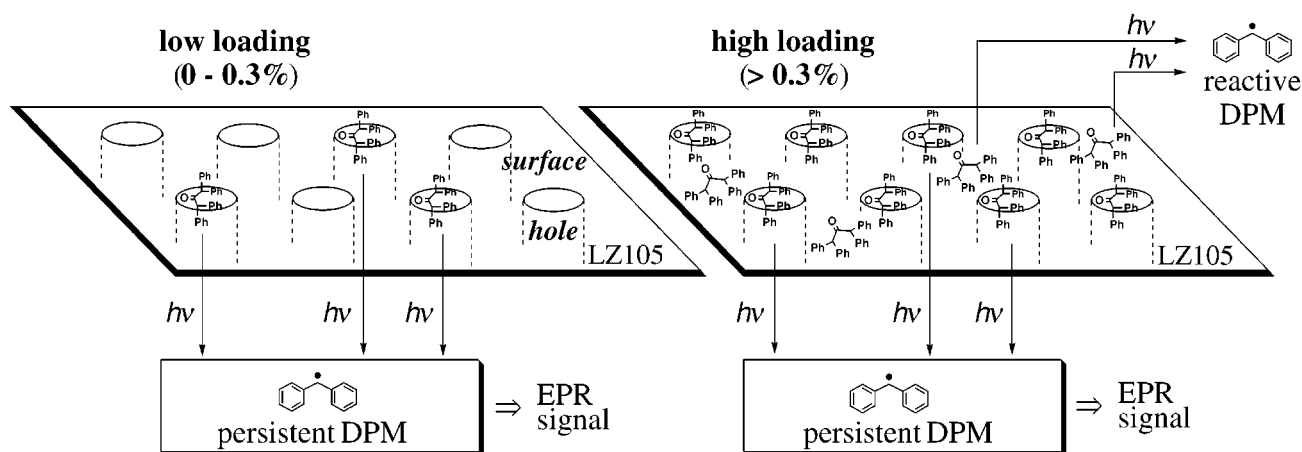
LZ-105 from an isooctane solution. The following qualitative features are apparent from Table 3. (1) Molecules whose steric cross sections allow access to the internal surface (*p*-xylene and acetophenone) showed an *M* value over 4 mg on 100 mg of LZ-105, a large amount of adsorption consistent with entry into the extensive internal surface. (2) Molecules whose steric cross sections are too bulky to allow access to the internal surface (*o*-xylene, triphenylmethane, and 2'-methylacetophenone) showed an *M* value below 0.6 mg on 100 mg of LZ-105, a value consistent with the formation of a monolayer on the external surface which was estimated and measured to have a surface area of ca. 15 m²/g. (3) Carbonyl-containing compounds tend to have a larger *M* value than that of a corresponding hydrocarbon compound of a similar molecular size, e.g., the *M* value of acetophenone is larger than that of *p*-xylene. (4) The maximum adsorbed amount (1.4 mg/100 mg of LZ-105) of diphenylmethane observed in Figure 9c is much larger than the *M* value of 2'-methylacetophenone, although diphenylmethane has no carbonyl group, consistent with internal adsorption.

Discussion

For **1** and **3** the results of computations, surface area measurements, photochemical product analysis, EPR analysis and adsorption isotherms are all consistent with the expectations of Schemes 1 and 2. It is assumed that these ketones are initially adsorbed in the holes (**M_h**/LZ-105) of the external surface until ca. 0.3–0.5% loading and then on the external framework (**M_f**/LZ-105), until a monolayer is formed at ca. 1% loading, and that photolysis of these distinct supramolecular isomers produces different supramolecular DPM radicals, **DMP_h** and **DMP_f**.

Scheme 3 depicts the situation schematically. The photoreaction of **1** generates two DPM radicals on the

Scheme 4



external surface; one of the radicals intercalated in a hole on the surface (DPM_h) is predisposed to diffuse into the internal surface, and the second radical of the pair (DPM_i) becomes detached from its partner and diffuses relatively freely on the external surface to form **2** in ca. 40–45% yield. This is reasonable, since at ca. 0.3–0.5% loading, most of the holes on the external surface are likely to remain filled by M_h until very high conversions are achieved. Since there is no evidence for a rapid disappearance of DPM on the time scale of the EPR experiments (minutes), we conclude that the combination reactions of DPM on the external surface are completed in the time scale of minutes. The time scale of adsorption of diphenylmethane, an isosteric analogue of DPM, is relatively slow (Figure 9b), supporting the conclusion that any radicals produced on the external surface are much more likely to undergo radical–radical reactions on the external surface, which provides no significant steric constraints to diffusion or radical–radical coupling.

The DPM_h radicals that diffuse essentially quantitatively into the internal surface are strongly persistent and exhibit a readily measured EPR spectrum (Figures 2 and 3). Addition of air to the sample results in rapid oxidation by oxygen to produce peroxy radicals that are readily detectable by EPR (Figure 2).

The following lines of reasoning provide further support for the proposed models of Schemes 1–3. The product analysis of the photoreaction of **1** adsorbed on LZ-105 showed that up to ca. 0.5% loading the yield of **2** is essentially constant at ca. 40–45% and is independent of irradiation time. This result indicates that approximately half of the DPM generated by the photoreaction of **1** leads to the radical coupling reaction to produce **2**, and the remaining DPM diffuses to the internal surface and becomes persistent (Scheme 4). This conclusion is further supported by quantitative EPR analysis which demonstrated that DPM is produced in ca. 50% yield. Above the point at which all holes are filled, the yield of **2** is expected to increase. Indeed, there is an increase in **2** from ca. 40–45% to ca. 50–60% above ca. 0.5% loading, the composition at which the holes on the external surface are filled with **1**.

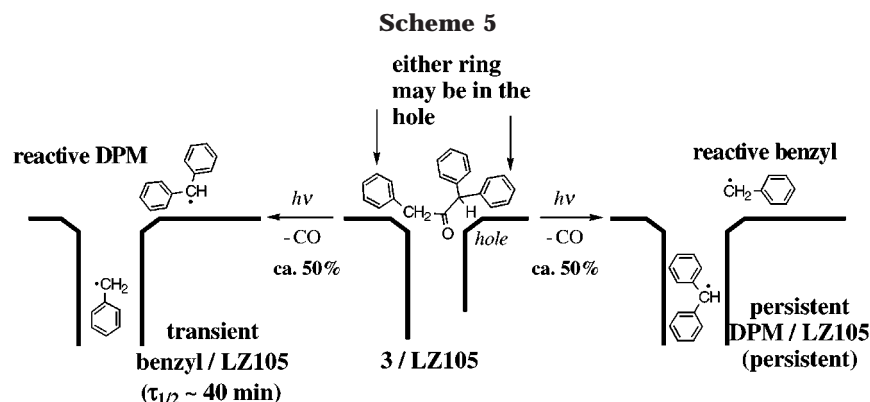
Basis for Persistence of DPM/LZ-105. Immobilization or Steric Effect on Radical–Radical Reactions? DPM radicals that are adsorbed into the internal surface are remarkably persistent, demonstrated by the fact that the EPR spectrum of **1** lasts for weeks. This

persistence demands that any radical–radical reactions are strongly inhibited when the DPM radicals are adsorbed in the internal surface. Two mechanisms can produce persistence: (1) immobilization and spatial separation of the radicals once adsorbed on the internal surface, and (2) mobility of the radicals, but inhibition of radical–radical reactions due to a supramolecular steric effect as the radicals approach each other.

Photolysis of **3** produces a DPM radical and a benzyl radical. From a quantitative analysis of the EPR results, it was concluded that there is no difference in the initial amounts of DPM and benzyl radicals produced by photolysis of **3** adsorbed into the internal surface. These results suggest that there is no significant radical size selectivity for DPM or benzyl radicals with respect to the probability of adsorption into the internal surface by DPM or BZ (Scheme 4). This conclusion, in turn, suggests that DPM radicals can diffuse in the internal surface and are not immobilized. In addition, the relative sharpness of the EPR spectrum of DPM is similar to that for other radicals (such as the α -methyl benzyl radical¹⁷) which have been shown unambiguously to undergo inhibited but finite reaction on the internal surface. Thus, although circumstantial, the evidence favors a certain mobility of the DPM radicals.

Product analysis of the photoreaction of **3**/LZ-105 showed that **2**, **4**, and **5** are formed in the ratio of 2:4:5 (4:13:5), which is comparable to the product ratio obtained by the photoreaction of **3** in *n*-hexane. From this we conclude that the low yield of radical coupling products was mainly formed on the external surface of LZ-105 where free diffusion, analogous to solution, can occur.

The time-course of the generation of DPM on LZ-105 (Figure 4) was monitored by EPR and provides kinetic evidence supporting the model. Dependence of the yield of DPM produced by photolysis of **1**/LZ-105 on the percentage of loading of **1** indicates that the supramolecular structure of **1**/LZ-105 changes at ca. 0.5% loading (Figure 5). This demonstrates a correlation between the site location of **1** adsorbed on the LZ-105 surface and the yield of persistent DPM occurring until ca. 0.5% loading, the composition that corresponds to the loading at which the holes on the external surface are filled. Above ca. 0.5% loading, the holes are all filled by 1_h /LZ-105, and the excess of **1** beyond 0.5% will be adsorbed on the external surface (Scheme 4) to form 1_e /LZ-105, where both



DPMs generated from one molecule of **1** have sufficient mobility to lead to the radical coupling reaction. In the case of 90 min irradiation (Figure 5c), the slope above 0.3–0.5% loading is steeper than that for shorter irradiation times. This result indicates that under “high” loading (>0.5%) and long irradiation conditions (hours), more persistent DPM radicals can be generated than the number of holes on the LZ-105 surface because each channel can contain more than one DPM_i. The explanation of this result is that the persistent DPM radicals generated at an early time of irradiation diffuse away from their initial site in a hole into the internal surface, generating a hole that is available for adsorption by DPM produced by photolysis of **1** adsorbed on the solid external surface (Scheme 4).

Comparison of the Photochemical Results with the Langmuir Isotherms. We will now show that the results of computation, photochemical, and EPR all correlate with the results of the Langmuir isotherm analysis and the evaluation of the surface area of the LZ-105 particles. The isotherms of **1** and its related compounds **3**, **6**, and **7** could be fit by a two-site Langmuir isotherm analysis. The Langmuir constant (k_i) of site I is about one hundred times larger than that of site II (Table 2a), indicating that **1** binds much more strongly to site I than to site II. The maximum adsorption amount (M_i) of **1** at site I of LZ-105 (100 mg) was estimated to be 0.3 mg, i.e., 0.3–0.5% loading by weight. The same value of ca. 0.3–0.5% loading matches the value of the maximum adsorption in the hole obtained by the time-course dependence (Figure 5) of the generation of DPM from the photoreaction of **1**/LZ-105. Therefore, from computations, photochemical and EPR analysis, and Langmuir analyses, we can confidently assign site I to a hole on the external surface, and site II to the solid external surface.

From the value of the estimated and measured external surface area of LZ-105 ($15 \text{ m}^2 \text{ g}^{-1}$), the number of holes available for adsorption is estimated to be sufficient to ca. 0.4 mg per 100 mg of LZ-105, in excellent agreement with the estimation of the loading at which all the holes are filled with **1** from the photochemical results, and further supporting the assignment of site I as a hole on the external surface. The amount of adsorbed amounts of **1**, **3**, **6**, and **7** in Table 2a is given in wt/wt units (mg per 100 mg of LZ-105). These units are not useful in expressing the fact that the system involves surface area as a critical dimension for expressing the number density of holes. To emphasize the importance of the surface area, the data in Table 2b is expressed in terms of another unit, mole per unit surface area ($= 245 \text{ \AA}^2$). The surface-normalized constants M_i , M_{iI} , k_i , and k_{iI} are summarized

in Table 2b. The normalized values of M_i for **1** and **3** are approximately one, strongly suggesting that one molecule each of **1** and **3** are adsorbed in the holes in a 1 to 1 stoichiometry on the external LZ-105 surface. In summary, we have convincing evidence from the photochemistry and Langmuir analysis that the bulky molecules are first strongly adsorbed in the holes (site I). After the holes are filled at ca. 0.3–0.5% loading, these molecules are more weakly adsorbed on site II, the solid external surface between the holes as shown in the paradigm of Schemes 1 and 2.

Summary and Conclusions

To characterize the external surface of a MFI zeolite, we have applied computations, photochemical probes, Langmuir isotherms, and EPR to support the paradigms shown in Schemes 1–5. From both computations and experiment, it is concluded that the holes on the external surface provide sites for up to ca. 0.3–0.5% loading of **1**. The filling of the holes constitutes stage I of Scheme 1 and produces a supramolecular structure that can be termed $\mathbf{1}_h/(\text{LZ-105})_{\text{ex}}$. During this stage, the photoreaction of **1** yields two DPM radicals that may be termed $\mathbf{1}_h/(\text{LZ-105})_{\text{ex}}$ and $\mathbf{1}_f/(\text{LZ-105})_{\text{ex}}$, i.e., one radical is produced in the hole on the external surface and the other is produced on the solid external surface.

For stage II, after the holes are filled, further addition of **1** results in adsorption on the solid external framework surface between the holes. Photoreaction of the molecules on the solid external framework surface also yields two DPMs, but in this case both of the radicals have mobility and rapidly undergo radical coupling on the external surface. As photolysis proceeds to higher conversion, and some holes become vacant, one of the two freely diffusing radicals produced from photolysis of **1** adsorbed on site II may diffuse into a vacant hole and become persistent. The maximum adsorption amounts of dibenzyl ketone derivatives **1**, **3**, **6**, and **7** of stage II are estimated by the addition of M_i and M_{iI} of Table 2. The values of $M_i + M_{iI}$ are in the range of 0.8–1 mg per 100 mg of LZ-105, consistent with the formation of a monolayer that is independent of structure. Thus, these results strengthen the paradigm and demonstrate, through a novel method, that the persistent radical probe and Langmuir isotherm analysis are practically useful for characterizing the external surface of MFI zeolites.

Completely persistent DPM at room temperature under degassed conditions was obtained by the photore-

action of **1** and **3** on the external surface of LZ-105, and the generation of DPM was easily observed by EPR. The reason for the persistence of DPM is explained by the transfer of DPM from a hole to the channel structure of LZ-105. The channel system of LZ-105 provides the *supramolecular steric effect* on DPM, in which DPM maintains its mobility. The amount of DPM photochemically generated from **1** is dependent on the coverage of the holes, which are filled by 0.3–0.5% loading of **1**. The Langmuir isotherm analyses of dibenzyl ketone derivatives show the existence of two adsorption sites on the external surface of LZ-105, with the adsorption property of one site being stronger than that of the other. The strong adsorption site is assigned as the hole, and the other site is assigned as the external framework surface between the holes. The Langmuir isotherm analysis also supports the fact that the holes are filled up by 0.3–0.5% loading of **1**, and the entire surface is covered by ca. 1% loading of **1**, quantitatively. Characterization of the LZ-105 particles also supports the coverage of the holes by **1** as the first adsorption step. These results strengthen the paradigm of Scheme 1 as the adsorption event of an organic molecule on the external surface of MFI zeolites.

Experimental Section

General Methods. LZ-105 (Si/Al = ca. 20) obtained from Union Carbide Co. was calcined at 500 °C in air more than 24 h before use. Isooctane of spectrophotometric grade (Aldrich) was used for adsorption experiments. EPR spectra were measured at room temperature. ¹H NMR spectra were recorded at 200 MHz. UV absorption spectra were obtained on a spectrophotometer. GC analyses were carried out using a chromatograph equipped with a flame ionization detector, a data station, and a capillary column (25 m × 0.2 mm).

Preparation of Tetraphenylacetone 1. To a solution of diphenylmethane (5.0 g, 30.0 mmol) in anhydrous THF (80 mL) was added 20 mL of 1.6 M *n*-butyllithium (32 mmol) in *n*-hexane at room temperature under Ar.²⁹ After stirring the red-colored mixture for 24 h at room temperature, the solution was cooled to –80 °C. Diphenylacetyl chloride (3.0 g, 11.5 mmol) in anhydrous THF (10 mL) was added to the cooled solution, and the reaction mixture was stirred at room-temperature overnight. The reaction was quenched in a saturated NaCl aqueous solution (50 mL), and the product was extracted with ether (400 mL). The ether layer was washed with brine and dried with Na₂SO₄. After removing the solvent, the residue was recrystallized from methanol/ethyl acetate, to give 2.5 g (54%) of **1** as a colorless powder; mp. 135–135.5 °C (lit.³⁰ 133–134 °C); EIMS *m/z* 362 (M⁺, 3), 195 (7), 167 (100); ¹H NMR (200 MHz, CDCl₃) δ 5.25 (s, 2 H) and 7.10–7.36 (m, 20 H); IR (KBr) 1709 cm⁻¹; UV λ_{max} (ε) 298 (338) and 260 (1010) nm in CH₃CN, 300 (334) and 260 (955) nm in isooctane.

Preparation of Triphenylacetone 3. Diphenylmethyl-lithium was prepared from diphenylmethane (5.0 g, 30.0 mmol) and *n*-butyllithium (32 mmol). To a solution of diphenylmethyl-lithium at –80 °C was added phenylacetyl chloride (2.0 g, 13 mmol) in anhydrous THF (8 mL), and the mixture was stirred at room-temperature overnight. The reaction was quenched in a saturated NaCl aqueous solution (50 mL), and the product was extracted with ether (300 mL). The ether layer was washed with brine and dried with Na₂SO₄. After the solvent was removed, the residue was purified by a silica gel column chromatography and recrystallization from methanol, to give 0.96 g (26%) of **3**³¹ as a colorless powder: mp 81–82 °C; EIMS *m/z* 286 (M⁺, 8), 167 (100), 165 (25), 91 (19); ¹H NMR

(200 MHz, CDCl₃) δ 3.79 (s, 2 H), 5.22 (s, 1 H) and 7.10–7.35 (m, 15 H); IR (KBr) 1709 cm⁻¹; UV λ_{max} (ε) 300 (319) and 260 (698) nm in isooctane.

Photoreaction of 1 in *n*-Hexane. A solution of **1** (101 mg, 0.279 mmol) in *n*-hexane (650 mL) was irradiated by using a 450 W medium-pressure mercury lamp for 30 min under Ar. After evaporating the solvent, the yellow residue was purified by using TLC (silica gel, CH₂Cl₂), to give 93.4 mg (100%) of tetraphenylethane **2** as a colorless powder; **2**; colorless cubes (from ethyl acetate); mp. 207–207.5 °C (lit.³² 211–212 °C); EIMS *m/z* 334 (M⁺, 2), 167 (100); ¹H NMR (200 MHz, CDCl₃) δ 4.77 (s, 2H) and 6.95–7.20 (m, 20H).

Preparation and Photoreaction of 1 Adsorbed on LZ-105. From the UV absorption measurement of the supernatant of **1** and LZ-105 mixture in isooctane, it was established that an adsorption of **1** on LZ-105 reached equilibrium in 40 min as shown in Figure 6. To a stock solution of **1** with a known concentration in isooctane was added 100 mg or 200 mg of LZ-105, and the suspension was stirred for 1 h at room temperature. Excess isooctane was evaporated with an Ar stream. The zeolite sample was transferred to a quartz vessel followed by evacuation with a vacuum line to ca. 5 × 10⁻⁵ Torr overnight. The evacuated sample was irradiated by a medium-pressure lamp (450 W) being tumbled for an appropriate time. After irradiation, the sample was exposed to air, and the products were extracted with 2–3 mL of THF containing methanol (5% v/v) overnight. The suspension was filtered and evaporated to give a residue containing **1** and products. The residue was dissolved in 1–3 mL of ethyl acetate, and 2-ethylnaphthalene (1 μL/1 mL of ethyl acetate) was added to the solution as an internal standard for GC. For GC analysis, the individual response factors of **1**, **2**, and benzophenone to 2-ethylnaphthalene were determined under the following conditions (injector; 280 °C, oven temperature; from 150 to 250 °C). Recovery of **1** and the yield of **2** and benzophenone were obtained by using their response factors as shown in Table 1.

For characterization of a radical with EPR, the samples were prepared in a quartz tube with a branch quartz tube for EPR measurement. The evacuated sample was irradiated using a lamp with tumbling for an appropriate time and was put in the EPR spectrometer's cavity at room temperature. After the EPR measurement, the procedure of irradiation and EPR measurement was repeated for tracing the generation of DPM.

Photoreaction of 3 in *n*-Hexane and on LZ-105. A solution of **3** (1.77 × 10⁻³ mol L⁻¹) in *n*-hexane (3 mL) was irradiated using a 450 W medium-pressure mercury lamp for 1 min under degassed conditions. After evaporating the solvent, the residue was dissolved in 1 mL of ethyl acetate, and 1 μL of 2-ethylnaphthalene was added to the solution as an internal standard for GC. Before GC analysis, the individual response factors of triphenylacetone **3**, ethane derivatives **2**, **4**, and **5**, and benzophenone to 2-ethylnaphthalene were determined. The recovery of **3** and the yields of products were obtained by GC with their response factors.

In the case of the photoreaction of **3** adsorbed on LZ-105, the samples of **3** adsorbed on LZ-105 were prepared in a manner similar to that of **1**. A zeolite sample of **3** in a quartz vessel under vacuum was photolyzed using a medium-pressure mercury lamp (450 W) and tumbling the vessel for 5 min. After exposing the sample to air, products were extracted with 3 mL of THF containing methanol (5% v/v) and were analyzed by GC using 2-ethylnaphthalene as an internal standard.

Adsorption Time-Course of 1 and Its Related Compounds on LZ-105 from an Isooctane Solution. To a 3 mL solution of **1** and its related compounds in isooctane with a definite initial concentration, 100 mg of LZ-105 was added, and the suspension was stirred at room temperature. After an appropriate time, the mixture was centrifuged for 1 min, and the UV absorption of the supernatant was measured for determining the amount of **1** and its related compounds left in the solution.

Langmuir Isotherm Analysis of 1 and Its Related Compounds on LZ-105. LZ-105 (100 mg) was added to a 3 mL solution of **1** or its related compounds with various

(29) (a) Wright, B. B.; Platz, M. S. *J. Am. Chem. Soc.* **1984**, *106*, 4175–4180. (b) Zieger, H. E.; Angres, I.; Mathisen, D. *J. Am. Chem. Soc.* **1976**, *98*, 2580–2585.

(30) Dean, D. O.; Dickinson, W. B.; Quayle, O. R.; Lester, C. T. *J. Am. Chem. Soc.* **1950**, *72*, 1740–1745.

(31) Hou, Z.; Takamine, K.; Aoki, O.; Shiraishi, H.; Fujiwara, Y.; Taniguchi, H. *J. Org. Chem.* **1988**, *53*, 6077–6084.

(32) Olah, G. A.; Surya Prakash, G. K. *Synthesis* **1978**, 397–398.

concentrations in isooctane, and the suspension was stirred at room temperature until the adsorption reached equilibrium. Most of the compounds, except *p*-xylene and acetophenone, were adsorbed for 1 h; *p*-xylene and acetophenone were adsorbed for 3 h. The suspension was centrifuged for 5 min. The absorption spectra of the supernatant and the initial solution were measured, and the amount of compound adsorbed on LZ-105 at equilibrium was determined from the absorption difference between the supernatant and the initial solution. Correlation between the amount (mg) of adsorbate left in a 3 mL solution and the amount (mg) of adsorbate adsorbed on 100 mg of LZ-105 at equilibrium was fitted using eqs 1 or 2 on a Macintosh computer employing the fitting routine of the graphic program Igor Pro, Version 3.12 for Macintosh (Wave Metrics, Inc.).

Acknowledgment. The authors thank the National Science Foundation for grant (NSF CHE-93-13102). This work was supported in part by the National Science Foundation and the Department of Energy under Grant No. NSF CHE-98-10367 to the Environmental Molecular Sciences Institute (EMSI) at Columbia University. The authors also thank Dr. Xuegong Lei for helpful discussions. The excellent technical assistance and suggestions of Mr. Zhiqiang Liu in preparing the cover graphic are gratefully acknowledged.

JO991298I